Journal of Alloys and Compounds 509 (2011) 3238–3245

Contents lists available at ScienceDirect

Journal of Alloys and Compounds

journal homepage: www.elsevier.com/locate/jallcom

Ab initio study of the structural, thermodynamic and electronic properties of the $Cu_{10}In_7$ intermetallic phase

S. Ramos de Debiaggi[a,b,*], G.F. Cabeza[b,c], C. Deluque Toro[a], A.M. Monti[d], S. Sommadossi[a,b], A. Fernández Guillermet[b,e]

[a] *Facultad de Ingeniería, Universidad Nacional del Comahue, Buenos Aires 1400, (8300) Neuquén, Argentina*
[b] *CONICET, Argentina*
[c] *Dpto. de Física, Universidad Nacional del Sur, Bahía Blanca, Argentina*
[d] *CNEA e Instituto Sabato (Univ. Nac. de San Martín/CNEA), Centro Atómico Constituyentes, Avda. General Paz 1499, B1650KNA, San Martín, Buenos Aires, Argentina*
[e] *Centro Atómico Bariloche e Instituto Balseiro, Avda. Bustillo 9500, (8400) Bariloche, Argentina*

ARTICLE INFO

Article history:
Received 20 September 2010
Received in revised form
25 November 2010
Accepted 14 December 2010
Available online 22 December 2010

Keywords:
Ab initio calculations
Transition metals and alloys
Cu–In and Cu–Sn intermetallic phases
Lead-free soldering alloys

ABSTRACT

The physico-chemical properties of the intermetallic phases in the Cu–In system have been a matter of considerable theoretical and experimental interest in connection with, *i.a.*, the application of In–Sn alloys as lead-free micro-soldering alloys. Recently, a new binary compound with the chemical formula $Cu_{10}In_7$ has been detected in a study of the η-phase field. The structure of the $Cu_{10}In_7$ phase has been determined as closely related to that of the $Cu_{11}In_9$ compound occurring in the phase diagram, but no experimental or theoretical information on its electronic structure, thermodynamic and equation-of-state properties has yet been reported. In the present work we report the lattice parameters, bulk modulus, energy of formation from the constituent elements and the electronic structure of the new phase, calculated by applying an *ab initio* density-functional-theory method. Our calculation technique uses the projector augmented wave potentials and the exchange-correlation functions of Perdew and Wang in the generalized gradient approximation. The present results for the $Cu_{10}In_7$ phase are compared with the experimental data available, and with the trends in structural and thermodynamic properties emerging from *ab initio* calculations also performed in the present study for various structurally related and neighboring compounds in the Cu–In phase diagram, *viz.*, the ideal $B8_2$–Cu_2In, $B8_1$–CuIn, $B8_2$–$CuIn_2$ phases and the $Cu_{11}In_9$ compound.

1. Introduction

The physico-chemical properties of the intermetallic phases (IPs) occurring in the Cu–In phase diagram have been the subject of recent theoretical and experimental studies in connection with the design of lead-free materials based on the Cu–In–Sn system to be used in diffusion soldering methods [1]. The investigation of the properties of the IPs formed at the interconnection zone is of great importance for defining the final properties of the joints. In particular, considerable effort has been devoted to the characterization of the η phase, which is one of the technologically relevant phases detected at the joint in diffusion couples [2]. The η phase is a common equilibrium phase of both the Cu–In [3] and Cu–Sn binary subsystems [4] of the Cu–In–Sn system, with equilibrium structures based on the B8 NiAs/Ni_2In family. In the Cu–In system η has an extended stability range both in composition (33–38 at.% In) and in temperature (up to $T = 940$ K) [3] and it is accepted that it involves at least two structures (Section 2).

Recently, a new phase with composition described by the formula $Cu_{10}In_7$ has been detected by Piao and Lidin [5] when investigating the Cu–In η-phase field. By X-ray diffraction analysis they determined that the $Cu_{10}In_7$ compound belongs to the monoclinic system and reported its lattice parameters and other structural data. However, no information is available about its electronic structure, the thermodynamic properties or the stability with respect to the neighboring Cu–In compounds that have been considered as stable phases in the Cu–In phase diagram. The general purpose of the present work is to provide such structural and thermodynamic information for the $Cu_{10}In_7$ compound using predictive theoretical methods.

When lacking reliable experimental data, *ab initio* methods become a very useful tool to gain information on the properties of stable, metastable or hypothetical phases of interest for the

* Corresponding author at: Dpto. de Física, Facultad de Ingeniería, Universidad Nacional del Comahue, Buenos Aires 1400, (8300) Neuquén, Argentina.
Tel.: +54 299 4490331; fax: +54 299 4490329.
E-mail addresses: sbramos@yahoo.com, ramos@uncoma.edu.ar (S. Ramos de Debiaggi).

0925-8388/$ – see front matter © 2010 Elsevier B.V. All rights reserved.
doi:10.1016/j.jallcom.2010.12.093

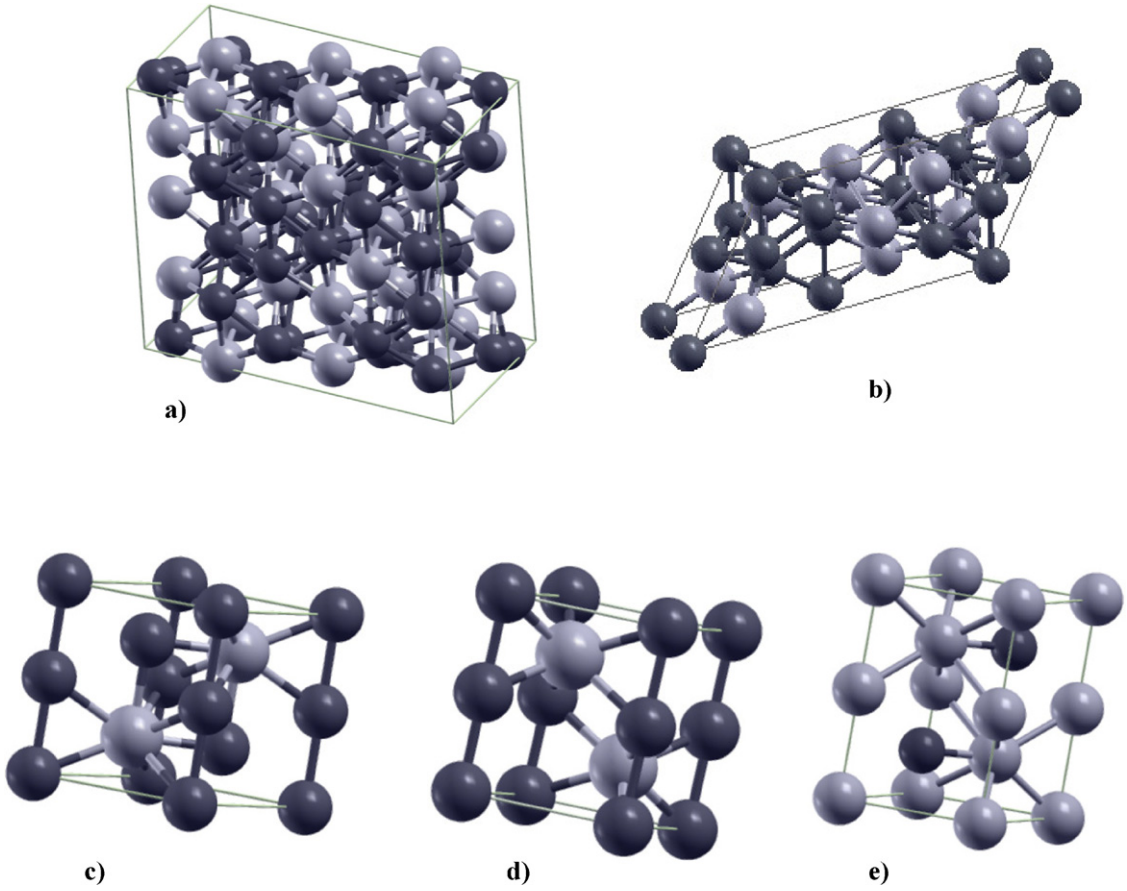

Fig. 1. Structures of the Cu–In intermetallic phases calculated in the present work: the monoclinic C2/m. (a) $Cu_{10}In_7$ (41 at.% In) and (b) $Cu_{11}In_9$ (45 at.% In) structures, and the ideal (c) $B8_2$–Cu_2In (33 at.% In), (d) $B8_1$–CuIn (50 at.% In) and (e) $B8_2$–$CuIn_2$ (67 at.% In) phases. Light grey and dark grey spheres represent In atoms and Cu atoms respectively.

understanding and the modelling of complex systems. In particular, *ab initio* methods might help to establish reliable trends in the frequently meager information on structural and phase stability properties of various kinds of compounds. In the present paper we report new *ab initio* calculations based on the density-functional theory (DFT) and the projector augmented-wave method (PAW) using the VASP code. Using these methods we study the structural and cohesive properties of the $Cu_{10}In_7$ phase and of various structurally related and neighboring compounds, *viz.*, the ideal phases $B8_1$–CuIn and $B8_2$–Cu_2In related to the η phase and the $Cu_{11}In_9$ phase.

In particular, for the $Cu_{10}In_7$ phase we report the electronic density of states, lattice parameters, bulk modulus and its pressure derivative, and the energy of formation. These results are compared with the values obtained *ab initio* for the ideal $B8_2$–Cu_2In, $B8_1$–CuIn, $B8_2$–$CuIn_2$ phases and the $Cu_{11}In_9$ compound. The present paper also includes a discussion of various open problems emerging from the suggestion that $Cu_{10}In_7$ might be a stable phase in the Cu–In phase diagram.

2. Phases and structures

The structures of the key compounds considered in this work are summarized in Fig. 1. $Cu_{10}In_7$ (Fig. 1a) is a monoclinic structure with C2/m symmetry group, consisting in a large cell with 40 Cu atoms and 28 In atoms. We adopted the experimental unit cell parameters: $a = 13.8463$ Å, $b = 11.8462$ Å, $c = 6.7388$ Å, and $\beta = 91.063^\circ$, and the atomic coordinates reported in [5] as input data in our calculations.

Piao and Lidin [5] noted that the structure of the $Cu_{10}In_7$ compound is closely related to that of $Cu_{11}In_9$ (Fig. 1b), which in addition is one of the two neighboring phases of the new compound in the Cu–In phase diagram. These facts suggest that $Cu_{11}In_9$ should also be included, as a reference, in an *ab initio* study of the recently discovered phase. $Cu_{11}In_9$ belongs to the monoclinic system C2/m, with a unit cell containing 20 atoms (*i.e.*, 11 Cu atoms and 9 In atoms) and lattice-parameters $a = 12.814$ Å, $b = 4.3543$ Å, $c = 7.353$ Å and $\beta = 54.49^\circ$ [6]. A detailed comparison of these structures was presented in Ref. [5]. Here we will only emphasize that in the new phase all the positions are fully ordered while in $Cu_{11}In_9$ the atomic sites at Wyckoff positions 2(d) have a mixed occupancy of Cu and In atoms. This feature was taken into account by us, when performing what seems to be the first *ab initio* study for the $Cu_{11}In_9$ phase. As a first approximation, the $Cu_{11}In_9$ phase was treated in a hypothetical, ordered state in which the 2(d) Wyckoff positions are occupied by one Cu atom and one In atom, respectively. Consequently, the translational (1/2, 1/2, 0) symmetry of the original C2/m point symmetry group is broken, and the actual symmetry of the compound as modelled here is reduced to P2/m point symmetry group.

Another natural reference to compare with the $Cu_{10}In_7$ results would indeed be the η phase, *i.e.*, the other neighboring phase of the new compound in the Cu–In phase diagram. However, the actual η-phase field shows a considerable structural complexity. In fact, a detailed description of the equilibrium structures of the η phase field in the Cu–In system has not yet been reported, although it is accepted that it involves at least two phases, *viz.*, a high temperature phase (HT-η or η′) and a low temperature phase (LT-η or simply η) [3]. The HT-η and LT-η phases have also been studied in the Cu–Sn binary subsystem [4]. These phases are monoclinic,

with known superstructures based on the NiAs–Ni_2In parent lattices [7]. Furthermore, it is also accepted that for the Cu–In system the NiAs–Ni_2In type structures are the basic arrangements upon which the complex superstructures observed are formed. At low temperatures even modulated structures have been detected for the η phases of the Cu–In system [8].

In view of the various problems involved in a realistic treatment of the actual Cu–In η phase, we included other reference structures in the present comparative *ab initio* study of the $Cu_{10}In_7$ phase, *viz.*, the Cu–In phases belonging to the ideal B8 NiAs/Ni_2In family. These compounds (Fig. 1c–e) constitute an important family of structures common to IPs formed between a transition metal element (T) and an element (B) of the groups III–VI in the Periodic Table [9], covering the whole range of compositions which goes from TB to T_2B. The basic $B8_1$ (P3/mmc) structure consists of an hexagonal compact lattice (Wyckoff positions 2(c): (1/3, 2/3, 1/4)) of the principal element (B) compressed along the *c* axis, with octahedral interstitial sites (2(a): (0, 0, 0)) occupied by the transition metal (T). In the variant $B8_2$ with higher content of T atoms, also trigonal bipyramid interstices are filled (sites 2(d): (1/3, 2/3, 3/4)). Both $B8_1$ and $B8_2$ structures are closely connected, in the $B8_1$ type the 2(d) sites are empty, while in the $B8_2$ these sites are completely filled. Superstructures are formed by incorporating ordered vacancies at the In(2c) and Cu(2d) positions in the $B8_1$–$B8_2$ structures. The properties of the ideal $B8_2$–Cu_2In, $B8_1$–CuIn, $B8_2$–$CuIn_2$ phases and the $Cu_{11}In_9$ compound were studied *ab initio* in the present work.

3. Theoretical method

Total energy DFT calculations were performed using the projector augmented-wave method (PAW) [10] and the VASP code [11]. We adopted the generalized gradient approximation for the exchange-correlation energy due to Perdew and Wang (GGA-PW91) [12]. The kinetic energy cut-off for the plane wave expansion of the electronic wavefunction was 314 eV. For the PAWs we considered 11 valence electrons for Cu ($3d^{10}4s^1$) and 3 for In ($5s^2p^1$). We used Monkhorst–Pack *k*-point meshes [13] and the Methfessel–Paxton technique [14] with a smearing factor of 0.1 for the electronic levels. The convergence of the *k*-point meshes was checked until the energy has converged with a precision better than 1 meV/atom. In this way the *k*-meshes considered were $7 \times 7 \times 11$ for $Cu_{10}In_7$, $3 \times 9 \times 5$ for $Cu_{11}In_9$, $17 \times 17 \times 13$ for the $B8_2$–Cu_2In and $B8_1$–CuIn ideal phases, and $19 \times 19 \times 11$ for the $B8_2$–$CuIn_2$ phase. These reciprocal lattice grids implied up to 286 *k* points in the irreducible part of the Brillouin zone (IBZ), depending on the structure. The criterion for the self-consistent convergence of the total energy was 0.1 meV. Taking the experimental unit cell data as input, the various structures studied in this work were fully relaxed with respect to their lattice parameters and the internal degrees of freedom compatible with the space group symmetry of the crystal structure, until the forces were less than 8 meV/Å and the energy variations with respect to the structural degrees of freedom was better than 1 meV/atom.

The energy of formation of the IPs was calculated as

$$\Delta E_f^{\phi}(Cu_mIn_n) = \frac{1}{m+n}E^{\phi}_{Cu_mIn_n} - \left[\frac{m}{m+n}E^{\theta}_{Cu} + \frac{n}{m+n}E^{\psi}_{In}\right] \quad (1)$$

where ΔE_f^{ϕ} is the energy of formation per atom for the Cu_mIn_n compound with the structure ϕ, $E^{\phi}(Cu_mIn_n)$ is the corresponding total energy, E^{θ}_{Cu} is the total energy per atom for pure Cu in its equilibrium phase θ (fcc), and E^{ψ}_{In} is the total energy per atom for pure In in its equilibrium phase ψ (tI2).

We calculated the total energy (E) and external pressure (P) for values of volume (V) varying slightly around the equilibrium (up to ±5%), relaxing all external and internal coordinates of the system. The bulk modulus (B_o) and its pressure derivative (B') were obtained by fitting the calculated values to the *P vs. V* relation given by the equation of state due to Vinet et al. [15], expressed as:

$$P = 3B_o x^{-2}(1-x)\exp[\chi(1-x)] \quad (2)$$

with $x = (V/V_o)^{1/3}$, V_o being the equilibrium volume, and $\chi = 3/2(B' - 1)$.

4. Results and discussion

In Table 1 we summarize the *ab initio* results for the constituent elements Cu and In in their known equilibrium structures, *i.e.*, fcc for Cu and tI2 for In, the ideal phases $B8_2$–Cu_2In, $B8_1$–CuIn and $B8_2$–$CuIn_2$, and for the IPs $Cu_{10}In_7$, $Cu_{11}In_9$. We report the lattice parameters, equilibrium volume, the bulk modulus and its pressure derivative, and the energies of formation with respect to the constituent elements. The present results for the elements are compared with available experimental data (see references listed at the footnote of Table 1), as well as our previously calculated values obtained using the DFT full potential linearized augmented plane wave (FP-LAPW) method as implemented in the Wien*2k* code [16]. The latter calculations were performed considering the GGA approximation and the Perdew–Burke–Ernzerhof-96 (PBE96) exchange-correlation functions [17]. For Cu we also include the results reported by Ghosh and Asta [18], calculated using ultrasoft pseudo potentials (US-PP) and the GGA approximation for exchange and correlation energy due to Perdew and Wang [19]. For In we also compare with the recent full-potential linear-muffin-tin-orbital (FP-LMTO) results reported by Sin'ko and Smirnov [20]. Although better agreement is found for other exchange-correlation functions tested in their work [20], in Table 1 we include their GGA-PW91 values, corresponding to the same exchange-correlation functions used in this work.

4.1. Cohesive properties of Cu and In

Our results for the lattice parameter and bulk modulus of Cu agree within less than 2% with the values from experiments [21–23] and with other calculated values (FP-LAPW and US-PPs). The calculated pressure derivative of the bulk modulus (B') is close to the corresponding US-PP reported value [18], although both theoretical predictions deviate appreciably from the FP-LAPW result, which presents the best agreement with the experimental values [24]. In the case of In it is found that the energy difference between the fcc and tI2 lattices is extremely small [16,25]. A *k*-point mesh larger than for the other systems considered in this work was required to favor the tI2 structure over the fcc one. Actually, by considering up to 2092 *k* points in the IBZ, the tI2 structure is stabilized with respect to fcc by only 0.4 meV/atom. The *ab initio* calculated lattice parameters of In agree within less than 2% with the experimental results at 291 K, and the calculated *c*/*a* ratio 1.524 compares excellently with the experimental value 1.523. However, the relative discrepancy between the theoretical and experimental B values for In is larger than for the other calculated properties, and we note that a similar trend in the discrepancy is found for the values calculated by using the FP-LAPW method in [16] and the FP-LMTO method in [20]. On the other hand, the B' value predicted here for In agrees well with the experimental result [26] and with the value obtained by using the FP-LMTO method in [20].

4.2. Structural parameters for the compounds

The structural parameters of the $B8_2$–Cu_2In, $B8_1$–CuIn and $B8_2$–Cu_2In phases obtained in the present DFT PAW calculations are in very good agreement with the results of our previous FP-LAPW work [16]. The agreement for the lattice parameters is better

Table 1
Calculated energies of formation, structural and elastic properties for Cu, In and Cu–In intermetallic phases at 0 K. The lattice parameters are given in Å, the equilibrium volume (V_o) in Å^3/atom, the bulk modulus (B_o) in GPa and the formation energies (obtained using Eq. (1)) in kJ/mol.

Phase	Space group	V_o	Lattice parameters	B_0	B'	ΔE_f
Cu-fcc	Fm3m	12.020	3.636	142.3	3.6	–
		(12.093)	3.644	139.1	(2.42)[a]	
		(11.932)	3.627	141.75	(5.17)[b]	
			3.596[c]	142[d]	(5.48, 5.04)[e]	
In-tI2	I4/mmm	27.512	a = 3.305, c = 5.036	36.4	4.7	–
		(27.553)	3.259, 5.190	34.9	(1.5)[b]	
		(27.395)	3.301, 5.028	36.7	(4.5)[f]	
		26.020[g]	3.245, 4.942[g]	41.8[h]	4.81[h]	
Cu_2In-$B8_2$	$P6_3/mmc$	15.534	a = 4.471, c = 5.384	92.1	4.7	7.631
		(15.513)	4.476, 5.364	102.9	3.1	(8.720)[b]
			(4.269, 5.239)[i] (4.292, 5.276)[j]			
CuIn-$B8_1$	$P6_3/mmc$	19.415	a = 4.250, c = 4.965	76.3	4.8	2.420
		(19.442)	4.260, 4.949	69.5	6.2	(4.387)[b]
$CuIn_2$-$B8_2$	$P6_3/mmc$	22.131	a = 4.606, c = 7.228	49.9	3.0	15.150
		(22.116)	4.605, 7.226	43.5	2.4	(16.772)[b]
$Cu_{10}In_7$	C2/m	16.841	a = 14.000, b = 12.047, c = 6.790, β = 90.00°	86.2	6.5	−1.744
		(16.251)	(13.845, 11.846, 6.739; 91.06)[k]			
$Cu_{11}In_9$	C2/m	17.369	a = 13.027, b = 4.406, c = 7.460 β = 54.22°	81.5	6.7	−0.825
		(16.697)	(12.814, 4.354, 7.353; 54.49)[l]			

[a] *Ab initio* US-PP, GGA-PW91 [18].
[b] *Ab initio* FP-LAPW, GGA-PBE96 [16].
[c] Experimental data extrapolated to 0 K [21,22].
[d] Experimental data at 0 K [23].
[e] Experimental data at 298 K [24].
[f] *Ab initio* FP-LMTO, GGA-PW91 [20]. The lattice parameters indicated here are deduced from their reported data.
[g] Experimental data at 291 K [6].
[h] Experimental data at 293 K [26].
[i] Experimental data for a sample at 35.6 at.% In [6].
[j] X-ray diffraction experimental data for a 36 at.% In sample, annealed at 773 K for 30 days [27].
[k] Experimental data for a sample annealed at 583 K for 9 months [5].
[l] Sample annealed at 553 K for 15 days [6].

than about 0.5%, although we note a larger discrepancy between the *ab initio* values for B differing up to 15% for the $CuIn_2$–$B8_2$ phase. The lattice parameters for $B8_2$–Cu_2In are compared with experimental values listed in Ref. [6] for a sample with a composition of 35.6 at.% In, and with the data obtained in our group [27]. Although the difference between theoretical and experimental values might be considered as acceptable also for this compound, we emphasize that the ideal $B8_2$–Cu_2In structure adopted in the calculations does not correspond to the actual structure of the η phase of the Cu–In phase diagram.

Our results show a very good agreement between theory and experiments for the lattice parameters of the $Cu_{10}In_7$ and $Cu_{11}In_9$ compounds. As expected, the *ab initio* GGA values tend to overestimate the lattice parameters of both compounds, with discrepancies between theoretical and experimental values of less than 2%. According to these results the optimum structure of the $Cu_{10}In_7$ compound, as obtained by globally relaxing the initial monoclinic structure, is closer to an orthorrombic lattice rather than to a monoclinic one, although the difference in the β angle is very small (less than 2%). In Tables 2 and 3 we present the optimized internal atomic coordinates of $Cu_{10}In_7$ and $Cu_{11}In_9$, respectively. Whereas in Table 3 we reproduce the original experimental symmetry information of the $Cu_{11}In_9$ compound, the actual internal coordinates here reported are splitted as a consequence of the symmetry breaking originated in the occupation of atomic sites 2d assumed in the calculation (Section 2). Even though the difference in the relaxations that take place for the splitted atomic positions is very small, strictly speaking, the actual point symmetry group of the modelled compound is P2/m.

In Fig. 2a and b, the volume per atom (V_o) and the bulk modulus (B_o) values obtained for the various compounds studied in the present work are plotted as a function of the In content. Results for the constituent elements are included as well as those for the ideal $B8_2$–Cu_2In, $B8_1$–CuIn and $B8_2$–$CuIn_2$ phases previously calculated by us using the FP-LAPW [16] method (the three crosses in the fig-

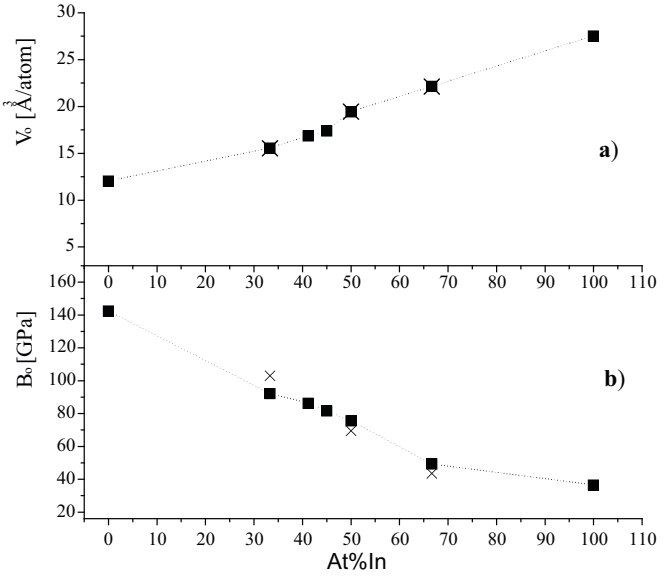

Fig. 2. Thermophysical properties of the Cu–In intermetallic phases calculated in the present work as functions of the atomic concentration of In: (a) the volume (V_o) per atom; (b) bulk modulus (B_o). Filled squared symbols correspond to values calculated in this work; the crosses correspond to the FP-LAPW results of Ref. [16]. The dashed lines are only guides to the eye.

Table 2
$Cu_{10}In_7$ unit cell internal coordinates (in Å) obtained from our *ab initio* calculations and experimental data from X-ray diffraction experiments for a sample annealed at 583 K [5].

Phase	Space group	Internal coordinates			
		Atom	Wyck.	(x, y, z): calculated	(x, y, z): experiment
$Cu_{10}In_7$	C2/m	In1	4i	0.16644, 0.00000, 0.49801	0.16663, 0.00000, 0.49713
		In2	4i	0.53476, 0.00000, 0.28229	0.53474, 0.00000, 0.28431
		In3	8j	0.69144, 0.22520, 0.19733	0.06864, 0.22601, 0.19841
		In4	4i	0.23688, 0.00000, 0.06623	0.23676, 0.00000, 0.06677
		In5	8j	0.34435, 0.22360, 0.38474	0.34438, 0.22418, 0.38721
		Cu1	8j	0.89279, 0.11029, 0.15463	0.89301, 0.11156, 0.15295
		Cu2	4e	0.25000, 0.25000, 0.00000	0.25000, 0.25000, 0.00000
		Cu3	8j	0.40484, 0.11276, 0.05941	0.40579, 0.11333, 0.06112
		Cu4	8j	0.70472, 0.11363, 0.27521	0.70448, 0.11267, 0.27500
		Cu5	4h	0.00000, 0.11107, 0.50000	0.00000, 0.11139, 0.50000
		Cu6	4i	0.35148, 0.00000, 0.39369	0.35125, 0.00000, 0.39244
		Cu7	4i	0.04883, 0.00000, 0.16516	0.04917, 0.00000, 0.16712

ures). The present results for the five studied compounds indicate a roughly linear variation of these thermophysical properties with the atomic concentration of In.

4.3. Electronic structure for the $Cu_{10}In_7$ and $Cu_{11}In_9$ intermetallic phases

In Fig. 3a and b we present the total and partial calculated electronic density of states (DOS) for $Cu_{10}In_7$ and $Cu_{11}In_9$, respectively. The DOS of both compounds looks very similar although the structure of peaks in the $Cu_{10}In_7$ main bonding band is rather more diffuse with respect to the corresponding one in the $Cu_{11}In_9$ phase. Both compounds show metallic behaviour at the Fermi level. The DOS per atom (given in states eV^{-1} $atom^{-1}$) at the Fermi level is relatively low for both phases, *viz.*, 0.25 for $Cu_{10}In_7$ and 0.21 for Cu_9In_{11}.

The most prominent bonding band of the DOS comes from Cu-d states, with a band width of approximately 2.5 eV which is completely occupied and located between −5 and −2 eV below the Fermi level. This band is around 1 eV narrower than the corresponding band in pure Cu (not shown here), a fact that can be attributed to the reduction of the number of Cu–Cu bonds and changes in the nearest-neighbor interatomic distances in the IPs with respect to those in the fcc Cu structure. In fact, considering a limiting distance of approximately 3 Å (between first and second neighbors of the Cu fcc lattice), the average coordination numbers (CNs) for both $Cu_{10}In_7$ and $Cu_{11}In_9$ compounds are similar, 10.80 and 10.91, respectively; and lower than the value (CN = 12) corresponding to the Cu fcc lattice. For $Cu_{10}In_7$ the average number of Cu–Cu and Cu–In bonds are both equal to 5.40; while for $Cu_{11}In_9$ these numbers are 4.73 and 6.18, respectively. The average nearest-neighbor distances are also very similar for both IPs, *viz.*, 2.77 Å for $Cu_{10}In_7$ and 2.74 for $Cu_{11}In_9$. These values are larger than the Cu–Cu nearest neighbor distance of the Cu fcc lattice which is 2.57 Å. At lower energies, between −10 and −6 eV approximately, the DOS has a free electron character, determined mainly by the contribution of Cu-s and In-s states that have a parabolic shape partial DOS. As the energy raises an increasing mixing of Cu-p and In-p states is observed.

In all the compounds studied here the Cu–In interactions shift the centroid of the d-band towards a higher binding energy (∼3.7 eV) in comparison with pure Cu.

4.4. Thermodynamic trends

The results in Table 1 indicate that the recently discovered monoclinic $Cu_{10}In_7$ compound and the $Cu_{11}In_9$ compound are thermodynamically stable with respect to the elements Cu and In in their stable structures at 0 K. The ideal $B8_2$–Cu_2In (33 at.% In), $B8_1$–CuIn (50 at.% In) and $B8_2$–$CuIn_2$ (67 at.% In) phases are shown to be thermodynamically unstable with respect to Cu and In at 0 K, in qualitative agreement with the results of our previous FP-LAPW calculations [16] also included in Table 1. The $B8_1$ phase, although unstable, is relatively more stable than the $B8_2$ structure. This is an interesting common trend found in *ab initio* studies of other closely related systems belonging to the B8 family of compounds, in particular, in the Cu–Sn [16,18] and Ni–In [16] systems. These trends are shown in Fig. 4, where the energy of formation obtained

Table 3
$Cu_{11}In_9$ unit cell internal coordinates (in Å) obtained from our *ab initio* calculations and experimental data from X-ray diffraction experiments for a sample annealed at 583 K [6]. Note that for the atomic site occupations assumed in the present work for Wyckoff positions (2d), the original translational symmetry (1/2, 1/2, 0) of the structure is broken (Section 2). The actual point symmetry group of the relaxed modelled compound reduces to P2/m.

Phase	Internal coordinates					
	Calculated			Experiment		
	Space group	Site	(x, y, z)	Space group	Site	(x, y, z)
$Cu_{11}In_9$	P2/m	In1:2m	0.13958, 0.00000, 0.16588	C2/m	In1:4i	0.1494, 0.0000, 0.1543
		In2:2n	0.65885, 0.50000, 0.14381			
		In3:2m	0.37533, 0.00000, 0.23792		In2:4i	0.3825, 0.0000, 0.2457
		In4:2n	0.88780, 0.50000, 0.25193			
		Cu1:1a	0.00000, 0.00000, 0.00000		Cu1:2a	0.0000, 0.0000, 0.0000
		Cu2:1e	0.50000, 0.50000, 0.00000			
		Cu3:2m	0.24987, 0.00000, 0.72139		Cu2:4i	0.2553, 0.0000, 0.7138
		Cu4:2n	0.76321, 0.50000, 0.71001			
		Cu5:2m	0.11458, 0.00000, 0.54408		Cu3:4i	0.1138, 0.0000, 0.5477
		Cu6:2n	0.61970, 0.50000, 0.55281			
		Cu7:1f	0.00000, 0.50000, 0.50000		M:2d	0.0000, 0.5000, 0.5000
		In5:1g	0.50000, 0.00000, 0.50000			

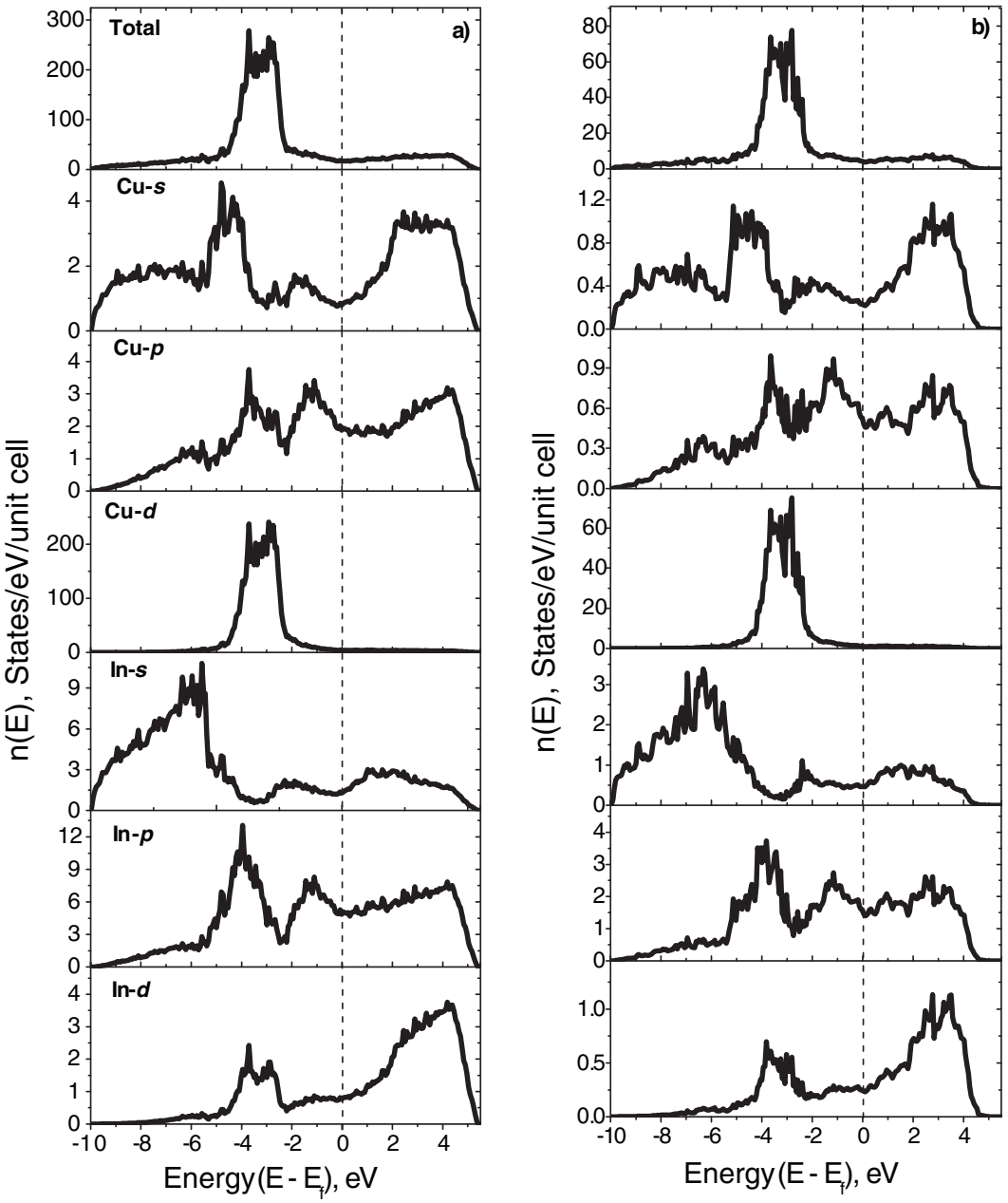

Fig. 3. Total and partial electronic density of states (DOS) for (a) $Cu_{10}In_7$ and (b) $Cu_{11}In_9$. The site decomposed DOS with their angular momentum, s, p and d band contributions, are plotted. The origin of the energy scale corresponds to the Fermi level.

for the various compounds studied in the present work are plotted as a function of the In content. For comparison, we include in this plot the FP-LAPW values for the ideal $B8_2$–Cu_2In, $B8_1$–CuIn and $B8_2$–$CuIn_2$ phases [16], as well as those for the Cu–Sn phases in the same composition range presented in Ref. [18]. Fig. 4 indicates that Cu–In compounds thermodynamically stable with respect to the constituent elements at 0 K should be expected to occur in a composition region extending from about 40 at.% In up to 45 at.% In. A similar trend is suggested by the Cu–Sn results [18], with the composition range for the thermodynamically stable compounds shifted to higher Sn contents.

4.5. Open problems on the stability of the $Cu_{10}In_7$ phase

The present study has made extensive use of DFT total energy calculations to establish trends in the relative stability of various Cu–In compounds with respect to the constituent elements at 0 K. On the other hand, the $Cu_{10}In_7$ compound was detected in experiments performed at 583 K, *i.e.*, a temperature at which the new phase is expected to coexist with other structures in the Cu–In phase diagram. There is no information available on the thermodynamic properties of the new phase which would allow, *e.g.*, a Gibbs energy analysis of the corresponding relative phase stability. In fact, the only source of information on the stability of the new phase relative to its neighboring phases is the work by Piao and Lidin [5]. In view of this general lack of information, it seems appropriate to close the present paper by discussing some of the questions emerging from assuming that the $Cu_{10}In_7$ compound is a stable phase in the Cu–In phase diagram.

In the first place, we note that the new phase might be related to the old φ phase (42 at.% In) which was included in an earlier version of the Cu–In phase diagram [28], but later replaced by the "line compound" $Cu_{11}In_9$. However, to the best of our knowledge no further reference to the φ phase has been made in the most

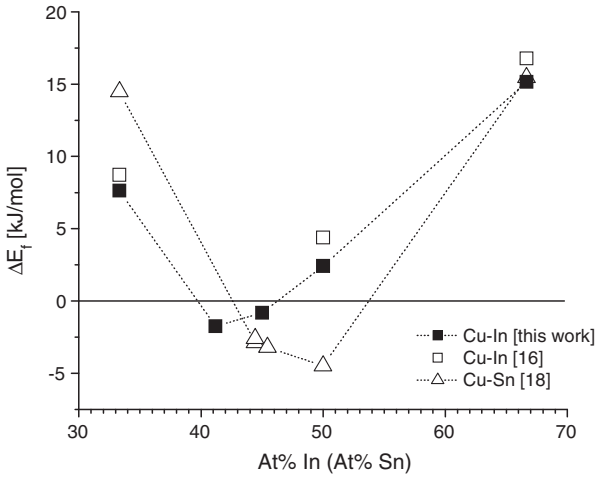

Fig. 4. Energy of formation of the ideal $B8_2$–Cu_2In, $B8_1$–CuIn and $B8_2$–$CuIn_2$ phases, the $Cu_{10}In_7$ and $Cu_{11}In_9$ compounds as a function of the atomic concentration of In obtained in the present work (filled squared symbols) and in Ref. [16] (open squared symbols). Open triangles correspond to calculated energies of formation for Cu–Sn compounds [18] plotted as a function of the Sn content. The dashed line is only a guide to the eye.

recent versions of the experimental Cu–In phase diagram [3].

The second issue concerns the relative stability of the various phases reported in the composition region of interest in the present study, *i.e.*, 30 < at.% In < 50. According to the most recent version of the Cu–In phase diagram three IPs are stable in that composition range, *viz.*, δ-Cu_7In_3 (30 at.% In), η-phase (33–38 at.% In) and $Cu_{11}In_9$ (45 at.% In), whereas the composition of the new phase (41.2 at.% In) falls between the η-phase field and the $Cu_{11}In_9$ compound. The new phase was detected by Piao and Lidin [5] in a sample with a nominal composition of 35.6 at.% In, annealed at 583 K for 9 months. By relying on the previously accepted phase diagram one would predict both η and $Cu_{11}In_9$ to be found in their experimental sample. However, this expectation is contradicted by two key observations reported by Piao and Lidin [5]. First, the $Cu_{11}In_9$ phase was not detected in the experimental alloy, and second, the $Cu_{10}In_7$ compound was found coexisting with small amounts of the neighboring δ-Cu_7In_3 rather than with the η phase.

The first observation together with a consideration of the similarities between $Cu_{10}In_7$ and $Cu_{11}In_9$ led Piao and Lidin [5] to suggest that $Cu_{11}In_9$ might not be a stable phase in the Cu–In phase diagram. In their view, the more disordered $Cu_{11}In_9$ compound might form first as a metastable phase, transforming into the more ordered $Cu_{10}In_7$ compound after long-time annealing. We note that in the current Cu–In phase diagram, based on the work by Bolcavage et al. [29], the $Cu_{11}In_9$ compound is considered as a stable phase down to room temperature.

The second observation by Piao and Lidin [5] opens up other questions about the stability of $Cu_{10}In_7$ relative to the η phase. In the first place, assuming that η is a stable structure in the Cu–In phase diagram remains to be understood why this structure was not detected after such a long-time annealing. A possible explanation is that the Gibbs energy of the η phase is higher than the one determined by the chemical potentials defined by the δ-Cu_7In_3 + $Cu_{10}In_7$ two-phase equilibrium. Alternatively, by taking into account the structural complexities of the η phase, which have been referred to before (Section 2), it seems reasonable to consider the possibility that $Cu_{10}In_7$ is not a distinct structure but belongs to the η phase field of the Cu–In phase diagram.

Various experimental and theoretical studies are in progress in our group which are aimed at clarifying these questions. In particular, starting with the phase stability trends at 0 K, the composition range treated in the present work (Section 4.4) will be extended down to 30 at.% In by performing new *ab initio* calculations for the Cu_7In_3 (δ-phase) compound. We close this section by emphasizing that in order to further correlate the *ab initio* results with the experimental phase stability observations made at finite temperatures, the vibrational entropy contribution to the Gibbs energy of the various Cu–In compounds should be accounted for.

5. Summary and conclusions

Using *ab initio* density functional calculations we have studied the structural, electronic and thermodynamic properties of the $Cu_{10}In_7$ compound, with a crystalline structure closely related to that of the $Cu_{11}In_9$ phase, which has recently been detected in a study of the η-phase field in the Cu–In phase diagram. With the *ab initio* density functional theory method, the PAW (projector augmented wave) potentials and the exchange-correlation potentials of Perdew and Wang in the generalized gradient approximation (GGA-PW91), we have calculated the lattice parameters, bulk modulus and its pressure derivative, the total energy, the electronic DOS and the energy of formation of $Cu_{10}In_7$ relative to the constituent elements. In addition, in order to study trends in the thermodynamic properties and the relative phase stability in the Cu–In system we have calculated the structural and thermodynamic properties of the $Cu_{11}In_9$ compound and various ideal hexagonal B8 NiAs/$InNi_2$ type phases, which are the base structures of those reported in the Cu–In η-phase field.

For the recently reported monoclinic $Cu_{10}In_7$ compound we calculate an energy of formation of −1.74 kJ/mol, indicating that the new phase is thermodynamically stable with respect to the constituent elements at 0 K. The $Cu_{11}In_9$ compound, as modelled in the present work, is also thermodynamically stable with respect to the constituent elements at 0 K, with an energy of formation of only 0.92 kJ/mol higher than the corresponding value for the $Cu_{10}In_7$ compound. For both intermetallic compounds the calculated structural parameters are in excellent agreement with the experimental information. According to our results the optimum structure for $Cu_{10}In_7$ is closer to an orthorrombic lattice rather than to a monoclinic one.

We found that the $B8_2$–Cu_2In, $B8_1$–CuIn and $B8_2$–$CuIn_2$ ideal phases are thermodynamically unstable with respect to the constituent elements at 0 K, with the $B8_1$–CuIn being relatively more stable that the $B8_2$–Cu_2In and $CuIn_2$ phases. This trend has also been observed in B8 compounds of other related systems, *e.g.*, in the Cu–Sn [16,18] and Ni–In [16] systems.

Concerning the electronic properties, the $Cu_{10}In_7$ and $Cu_{11}In_9$ compounds studied in the present work show metallic behaviour. For both intermetallic phases the band width of the total DOS is narrower by approximately 1 eV than the corresponding band width for pure Cu. This effect is attributed to both structural and chemical effects in the nearest neighbor atomic distributions. In all the compounds investigated, the presence of Cu–In interactions produces a shift of the centroid of the d-band towards higher binding energy (∼ 3.7 eV) with respect to that band in pure Cu.

Acknowledgements

This work was supported by Agencia Nacional de Promoción Científica y Tecnológica (BID 1728/OC-AR, PICT-2006 1947), Universidad Nacional del Comahue (Project I157), Universidad Nacional de San Martín (Project C057) and Universidad Nacional de Cuyo (SeCTyP, Project 1873). One of the authors (SRD) wish to thank Dr. V. Ganduglia Pirovano, from Instituto de Catálisis y Petroquímica – CSIC, for helpful suggestions concerning the VASP calculations; and Dr. M. Esquivel, from Centro Atómico Bariloche –

CONICET, for a enlightening discussion on symmetry properties of the modelled $Cu_{11}In_9$ phase.

References

[1] S.A. Sommadossi, Investigation on Diffusion Soldering in Cu/In/Cu and Cu/In48Sn/Cu Systems, Dissertation an der Universität Stuttgart, Bericht Nr. 125, 2002.
[2] S.A. Sommadossi, A. Fernández Guillermet, Intermetallics 15 (2007) 912–917.
[3] H. Okamoto, J. Phase Equilib. 5 (2) (1994) 226–227.
[4] N. Saunders, A.P. Miodownik, Bull. Alloy Phase Diagr. 11 (1990) 278–287.
[5] S. Piao, S. Lidin, Z. Anorg. Allg. Chem. 634 (2008) 2589–2593.
[6] P. Villars, Pearson's Handbook Desk Edition, ASM International, Materials Park, OH, 1997.
[7] A.K. Larsson, L. Stenberg, L. Lidin, Acta Crystallogr. B 50 (1994) 636–643.
[8] M. Elding-Pontén, L. Stenberg, S. Lidin, J. Alloys Compd. 261 (1997) 162–171.
[9] S. Lidin, A.K. Larsson, J. Solid State Chem. 118 (1995) 313–322.
[10] P.E. Blöchl, Phys. Rev. B 50 (1994) 17953–17979;
G. Kresse, J. Joubert, Phys. Rev. B 59 (1999) 1758–1775.
[11] G. Kresse, J. Furthmüller, Comput. Mater. Sci. 6 (1996) 15–50.
[12] J.P. Perdew, Y. Wang, Phys. Rev. B 44 (1991) 13298–13307.
[13] H.J. Monkhorst, J.D. Pack, Phys. Rev. B 13 (1976) 5188–5192.
[14] M. Methfessel, A.T. Paxton, Phys. Rev. B 40 (1986) 3616–3621.
[15] P. Vinet, J.H. Rose, J. Ferrante, J.R. Smith, J. Phys.: Condens. Matter 1 (1989) 1941–1963.
[16] S. Ramos de Debiaggi, A.M. Monti, C. Deluque Toro, S.A. Sommadossi, A. Fernández Guillermet, Estudio *ab-initio* de propiedades estructurales y termodinámicas de compuestos intermetálicos con estructuras B8: casos Cu–In y Cu–Sn, in: Proc. 9° Congreso Internacional de Metalurgia y Materiales, SAM-CONAMET V. II, 2009, pp. 1181–1186, http://www.cnea.gov.ar/samconamet2009.
[17] J.P. Perdew, S. Burke, M. Ernzerhof, Phys. Rev. Lett. 77 (1996) 3865–3868.
[18] G. Ghosh, M. Asta, J. Mater. Res. 20 (2005) 3102–3117.
[19] J.P. Perdew, Y. Wang, Phys. Rev. B 45 (1992) 13244–13249.
[20] G.V. Sin'ko, N.A. Smirnov, Phys. Rev. B 74 (2006) 134113–134120.
[21] M.E. Straumanis, L.S. Yu, Acta Cristall. A 25A (1969) 676–682.
[22] M. Kantola, E. Tokola, Phys. 223A (1967) 1–10.
[23] W.C. Overton Jr., J. Gaffney, Phys. Rev. 98 (1955) 969–977.
[24] D.J. Steinberg, J. Phys. Chem. Solids 43 (1982) 1173–1175.
[25] U. Häussermann, S.I. Simak, R. Ahuja, B. Johanson, S. Lidin, Angew. Chem. Int. Engl. 38 (1999) 2017–2020;
A.S. Mikhaylushkin, S.I. Simak, B. Johansson, U. Häussermann, Phys. Rev. B 72 (2005) 134202.
[26] K. Takemura, Phys. Rev. B 44 (1991) 545–549.
[27] C. Ararat-Ibargüen, S.A. Sommadossi, S. Ramos de Debiaggi, A.M. Monti, M. Esquivel, A. Fernández Guillermet, Estudio experimental de la influencia de la composición sobre la transición de fases en la región 33–37% at. In del sistema Cu–In, in: Proc. 9° Congreso Internacional de Metalurgia y Materiales, SAM-CONAMET V. I, 2009, pp. 715–720, http://www.cnea.gov.ar/samconamet2009.
[28] M. Hansen, K. Anderko, Constitution of Binary Alloys, McGraw Hill Company Inc., 1958.
[29] A. Bolcavage, S.W. Chen, C.R. Kao, Y.A. Chang, A.D. Romig Jr., J. Phase Equilib. 14 (1993) 14–21.